Cell PRESS
Open ACCESS

Cell Reports
Article

Innate Immune Messenger 2-5A Tethers Human RNase L into Active High-Order Complexes

Yuchen Han,[1] Gena Whitney,[1] Jesse Donovan,[1] and Alexei Korennykh[1,*]
[1]Department of Molecular Biology, Princeton University, 216 Schultz Laboratory, Princeton, NJ 08540, USA
*Correspondence: akorenny@princeton.edu
http://dx.doi.org/10.1016/j.celrep.2012.09.004

SUMMARY

2′,5′-linked oligoadenylates (2-5As) serve as conserved messengers of pathogen presence in the mammalian innate immune system. 2-5As induce self-association and activation of RNase L, which cleaves cytosolic RNA and promotes the production of interferons (IFNs) and cytokines driven by the transcription factors IRF-3 and NF-κB. We report that human RNase L is activated by forming high-order complexes, reminiscent of the mode of activation of the phylogenetically related transmembrane kinase/RNase Ire1 in the unfolded protein response. We describe crystal structures determined at 2.4 Å and 2.8 Å resolution, which show that two molecules of 2-5A at a time tether RNase L monomers via the ankyrin-repeat (ANK) domain. Each ANK domain harbors two distinct sites for 2-5A recognition that reside 50 Å apart. These data reveal a function for the ANK domain as a 2-5A-sensing homo-oligomerization device and describe a nonlinear, ultrasensitive regulation in the 2-5A/RNase L system poised for amplification of the IFN response.

INTRODUCTION

RNase L is a mammalian signaling protein that regulates the production of type I interferons (IFNs) in the innate immune system (Chakrabarti et al., 2011). RNase L is important for antiviral protection (Ireland et al., 2009; Jha et al., 2011), BRCA1- and IFNγ-mediated apoptosis (Mullan et al., 2005), prostate cancer suppression (Maier et al., 2005), and terminal differentiation of adipocytes (Fabre et al., 2012). RNase L is activated upon binding of a second messenger, 2-5A, that is produced by oligoadenylate synthetases (Hartmann et al., 2003; Sadler and Williams, 2008). The 2-5A/RNase L complex cleaves viral and cellular RNA, and activates the RIG-I-, MDA-5-, and NF-κB-mediated IFN response (Chakrabarti et al., 2011; Domingo-Gil et al., 2010; Jiang et al., 2011; Luthra et al., 2011; Malathi et al., 2007).

RNase L belongs to the family of >500 human kinases (Manning et al., 2002; Figure 1A). It contains a catalytically inactive pseudokinase domain (Silverman et al., 1988) and uses the enzymatic activity of its C-terminal endoribonuclease domain for signaling (Dong et al., 2001; Dong and Silverman, 1997; Figure 1A). RNase L has been shown to bind 2-5A with its N-terminal sensor, comprised of nine ankyrin repeats, and to form 2-5A-induced dimers (Chakrabarti et al., 2011; Cole et al., 1997; Dong and Silverman, 1995; Naik et al., 1998).

The structural basis of 2-5A binding to RNase L was established by the crystal structure of the sensor domain in complex with 2-5A (Tanaka et al., 2004). Paradoxically, this structure could not explain the mechanism of 2-5A-dependent RNase L dimerization because the sensor domain crystallized as a monomer (Tanaka et al., 2004). On the basis of this structure, it was proposed that 2-5A may regulate RNase L via a conformational change in the sensor domain (Tanaka et al., 2004). It was also suggested that the sensor domain may serve as a repressor of RNase L dimerization, and that 2-5A binding could derepresses the autoinhibited state of RNase L (Dong and Silverman, 1997). Here, we show that the sensor domain undergoes 2-5A-mediated self-association without conformational changes, and drives dimerization and high-order oligomerization of RNase L.

RESULTS

2-5A Promotes High-Order Homo-Oligomerization of RNase L

It was previously reported that 2-5A binding activates RNase L by inducing its dimerization (Dong and Silverman, 1995). However, high-order oligomerization and cooperative activation were recently demonstrated for a transmembrane homolog of RNase L, kinase/RNase Ire1, in the unfolded protein response (UPR) (Figure S1A; Korennykh et al., 2009). Because the subcellular localization (endoplasmic reticulum [ER] membrane versus cytosol), the physiological activators (polypeptides versus 2-5A), and the downstream transcriptional programs of Ire1 and RNase L are vastly dissimilar, we sought to determine the extent to which RNase L shares the signaling mechanism with Ire1, and whether RNase L forms signaling complexes larger than the dimer.

The formation of the catalytically active homo-oligomers of Ire1 became apparent from the highly cooperative activation profile of this kinase/RNase (Korennykh et al., 2009). Here, we employed a similar RNA cleavage readout to define the cooperativity of RNase L activation. We used the 5′-^{32}P-labeled RNA $C_{11}U_3C_7$ as a substrate of RNase L and observed rapid cleavage of this RNA at a single site, as reported previously (Carroll et al., 1996; Figure S1B). The RNase activity increased nonlinearly as a function of RNase L concentration and exhibited a cooperativity

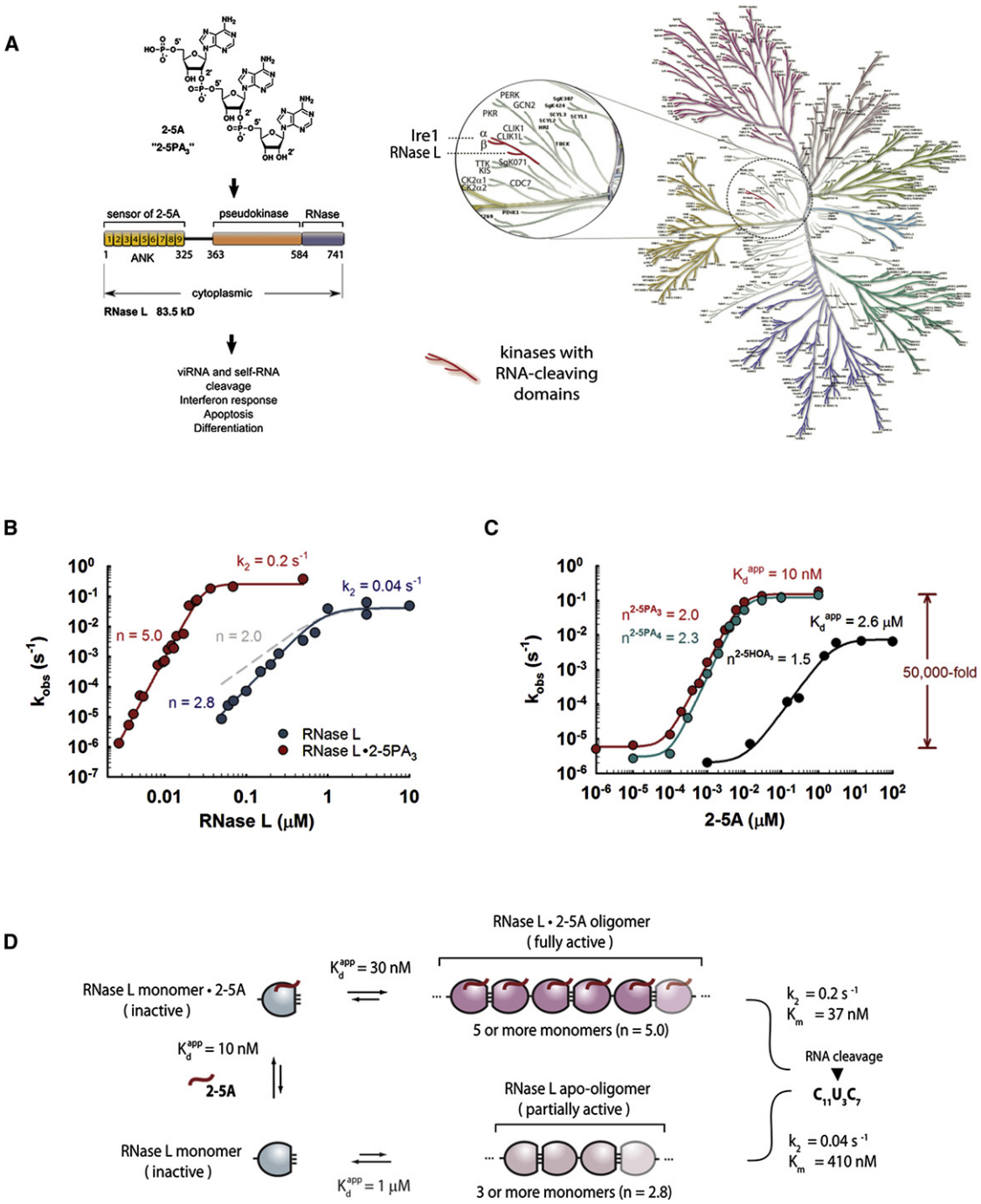

Figure 1. High-Order Assembly of RNase L Revealed by Cooperative Activation

(A) Left: Overview of the 2-5A/RNase L signaling system. Right: Position of RNase L in the human kinome (Manning et al., 2002). RNase L (cytosolic) is related to the kinase/RNase Ire1 (ER membrane resident) in the UPR.

(B) Cooperative activation of RNase L without (blue) and with (red) 2-5PA_3 (1 μM) present. The data were fit to a cooperative activation model with Hill coefficients n = 2.8 (without 2-5PA_3) and n = 5.0 (with 2-5PA_3; Experimental Procedures). A theoretical curve for n = 2.0 (dashed line) is provided for comparison.

(C) Cooperative activation of RNase L by three variants of 2-5A. Reactions contained 30 nM RNase L. Data were fit to a cooperative binding model (Experimental Procedures). Reactions were conducted at 20°C in buffer containing 20 mM HEPES (pH 7.4), 2 mM $Mg(OAc)_2$, 70 mM NaCl, 4 mM DTT, 10% glycerol, <1 nM ^{32}P-5′-$C_{11}U_3C_7$, and 2-5A as indicated.

(D) Kinetic framework for RNase L activation derived from the data in (B) and (C), and Figure S1. Two different oligomeric interfaces of RNase L are shown with one and three lines, respectively.

coefficient (n) of 2.8 (Figure 1B, blue circles), which is distinct from the cooperativity coefficient of the dimerization model with n = 2 (Figure 1B, dashed line). These data indicate that RNase L forms catalytically active complexes that contain three or more protomers. Unexpectedly, RNase L did not require 2-5A for activation, and at sufficient concentrations ($\geq$1 μM) exhibited high endoribonuclease activity.

In the presence of saturating concentrations of 2-5PA$_3$ (5′-P-A$_{2′,5}$A$_{2′,5′}$A), the endoribonuclease activity increased by ~10^4-fold (at 30 nM RNase L; Figure S1C). The same activity was measured when RNase L was preincubated with 2-5PA$_3$ for 15 s and for 23 min, suggesting that the activation kinetics is rapid. The cooperativity of the activation profile measured in the presence of 2-5PA$_3$ increased to n = 5 (Figure 1B, red circles), indicating that five or more monomers of the RNase L•2-5PA$_3$ complex associate to form catalytically active oligomers of RNase L.

To complete the basic characterization of RNase L, we examined its activation by 2-5A. The profiles for activation of RNase L by 2-5A were reported previously (Carroll et al., 1996; Cole et al., 1996). These studies revealed noncooperative responses, presumably because the experiments employed a narrow range of 2-5A concentrations and monitored only several-fold changes in rates. Here, we determined the activation profile of RNase L by titrating 2-5A concentrations to cover five orders of magnitude (Figure 1C). The activity of RNase L increased by ~10^4- to 10^5-fold upon addition of 2-5PA$_3$, 2-5PA$_4$ (5′-P-A$_{2′,5}$A$_{2′,5′}$A$_{2′,5′}$A), or 2-5HOA$_3$ (5′-HO-A$_{2′,5}$A$_{2′,5′}$A). The variants of 2-5A with 5′-phosphate, and three or four adenosines exhibited similar cooperativity (Hill) coefficients (n = 2–2.3) and activated RNase L with an apparent K$_d$ = 10 nM. The variant of 2-5PA$_3$ without the 5′-phosphate, 2-5HOA$_3$, activated RNase L partially (to ~1/20 of the maximum rate with 2-5PA$_3$ and 2-5PA$_4$), and exhibited ~260-fold weaker binding. The activation of RNase L by 2-5HOA$_3$ was cooperative, but with a smaller Hill coefficient n = 1.5. The high potency of 2-5PA$_3$ and 2-5PA$_4$ but not 2-5HOA$_3$ shows the importance of the 5′-phosphate for RNase L activation, in agreement with previous findings (Dong and Silverman, 1995). The structural analysis described below suggests that the 5′-phosphate group helps position 2-5A at the templating binding site of RNase L for recognition by the second, sensing binding site.

The quantitative measurements of the observed cooperative phenomena suggest a simple thermodynamic framework for activation of RNase L (Figure 1D). According to this framework, RNase L becomes activated in two modes, one dependent on 2-5A and the other independent of 2-5A. In both modes, RNase L assembles into a high-order, catalytically active complex. To form complexes larger than a dimer, RNase L is required to have at least two different oligomeric interfaces, as indicated in Figure 1D. In the presence of 2-5A, the assembly is more cooperative and requires lower concentrations of RNase L. The complex formed by RNase L with 2-5PA$_3$ bound exhibits higher specific activity (k_2 = 0.2 s^{-1} versus 0.04 s^{-1}) and stronger binding of the RNA substrate (K_m = 37 nM versus 410 nM; Figure S1D and S1E) than the complex formed by apo-RNase L, indicating that oligomers of RNase L•2-5PA$_3$ recognize the RNA substrate optimally.

Visualization of RNase L Oligomers by Chemical Crosslinking

To verify the high-order oligomerization of RNase L independently, we developed an assay to detect RNase L complexes in solution based on chemical crosslinking with glutaraldehyde (Cornell, 1989; Hayer-Hartl et al., 1995; Mischke et al., 1998). We began by examining whether we could detect high-order oligomers of Ire1 under the established conditions for oligomerization of its kinase/RNase module (Korennykh et al., 2009). To that end, we recreated the reaction mixture with Ire1KR32 and ADP as described previously (Korennykh et al., 2009), and supplied it with freshly dissolved glutaraldehyde (5 mM; Experimental Procedures). Upon analysis by Coomassie-stained gel, we observed monomers, dimers, trimers, and higher-order oligomers of Ire1 (Figure S2A). The dimer was resolved in two bands, possibly reflecting crosslinking of the same interface via different amino acids or crosslinking of different dimerization interfaces present in the high-order oligomer (Korennykh et al., 2009). The apparent abundance of larger oligomers versus dimer increased with time due to the higher probability of multiple crosslinks at longer incubations. A control protein, bovine serum albumin (BSA), reacted with glutaraldehyde, as indicated by the increased smearing of the bands over time, but remained monomeric (Figure S2B).

We extended the crosslinking analysis to RNase L. At low protein concentration (300 nM), monomer only (83.5 kD) was observed for full-length RNase L after 30 s of crosslinking, whereas dimers and trimers were visible after longer incubation (Figure 2A). Upon addition of 2-5PA$_3$ (1 μM), the crosslinking pattern changed noticeably. A pronounced band of RNase L dimer was detected after 30 s of crosslinking, whereas trimers and tetramers were apparent after 10 min. To better visualize the higher-order complexes, we increased the RNase L concentration to 3 μM (Figure 2B). High-order oligomers were observed after 20 s of crosslinking and dominated the sample after 13 min and 40 min. When the concentration of 2-5PA$_3$ was increased to match the concentration of RNase L (3 μM), high-order oligomers larger than dimers dominated the sample after 2 min of crosslinking (Figure S2C). The response of the crosslinking pattern to a specific ligand of RNase L, 2-5A, further indicates that crosslinking under the conditions used arises from specific RNase L complexes.

Next, we fixed the concentration of RNase L at 1 μM and titrated 2-5PA$_3$ between 100 nM (0.1 molar equivalents) and 5 μM (5 molar equivalents). The crosslinked sample of RNase L migrated predominantly as monomers at 100 nM 2-5PA3, and predominantly as dimers and high-order oligomers at 1 μM and 5 μM (Figure 2C). Therefore, increasing the 2-5PA$_3$ concentration when all other variables remain constant induces dimers and higher-order oligomers of RNase L, further supporting conclusions from the RNA cleavage readout.

Analysis of RNase L by size-exclusion chromatography in the absence of 2-5A revealed a single peak overlapping with dimer and monomer positions and migrating closer to monomer (Figure S2D). Upon addition of 2-5A, the peak shifted toward dimer and migrated over a size range corresponding to dimer (peak maximum), monomer, and trace amounts of larger complexes (Figure S2E). With increases in the protein and 2-5A

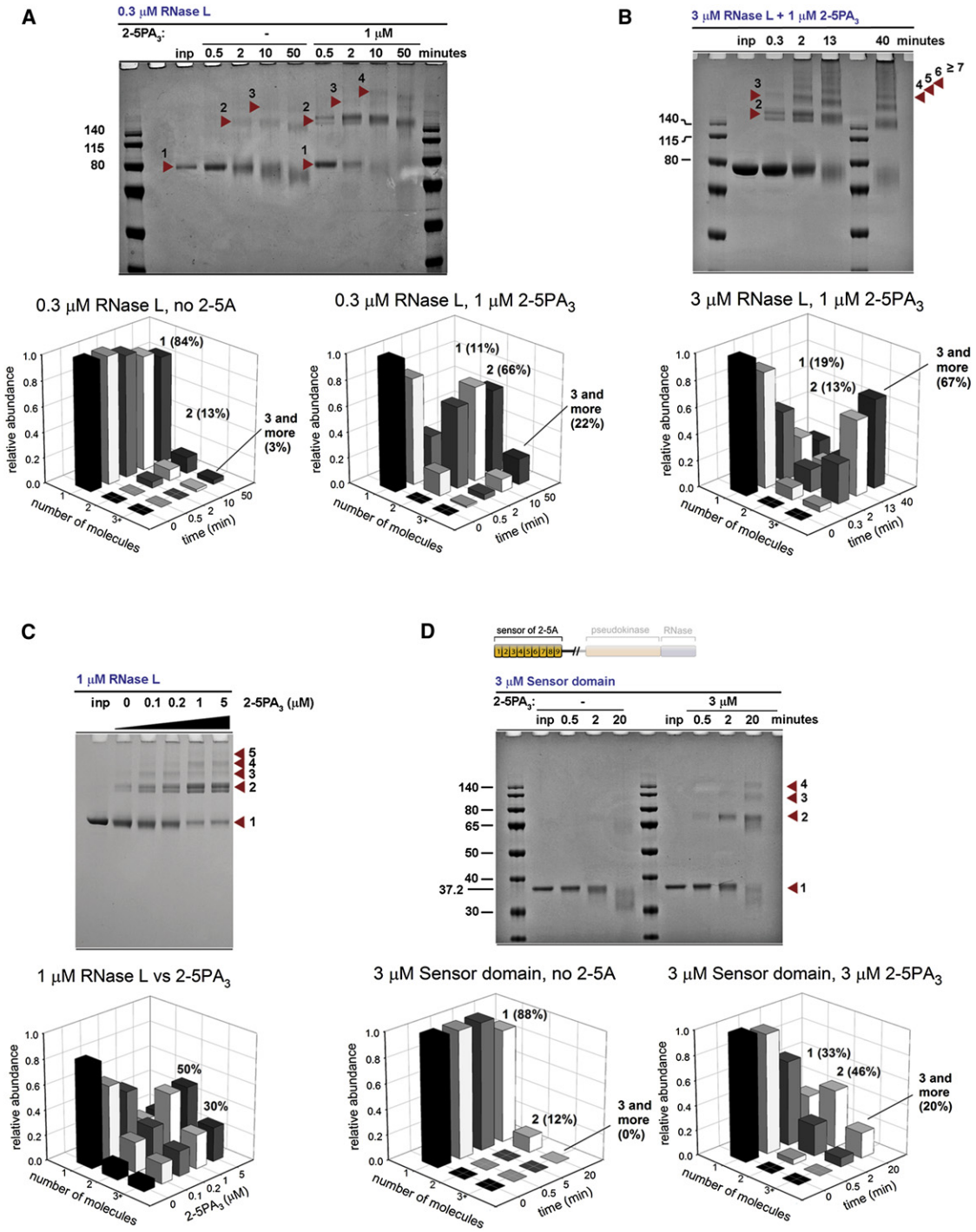

Figure 2. Visualization of RNase L Oligomers by Chemical Crosslinking

(A) Crosslinking of full-length RNase L (83.5 kD MW) at 300 nM concentration, in the absence or presence of 2-5PA$_3$.

(B) Crosslinking of full-length RNase L at 3 μM concentration, in the presence of 2-5PA$_3$ (1 μM). Crosslinking reactions were conducted in the same buffer as in Figure 1 and contained 5 mM glutaraldehyde. Bar charts show quantitation of the gels. Oligomer sizes were measured using the gel ruler in http://biochemlabsolutions.com/GelQuantNET.html software (Experimental Procedures).

(C) Induction of RNase L oligomers by 2-5PA$_3$. Crosslinking reactions were conducted for 10 min in the presence of 1 μM RNase L and 0-5 μM 2-5PA$_3$.

(D) Crosslinking of the purified sensor domain (3 μM; 37 kD MW) in the absence or presence of 2-5PA$_3$ (3 μM). Bar charts show quantitation of the gel. See also Figure S2.

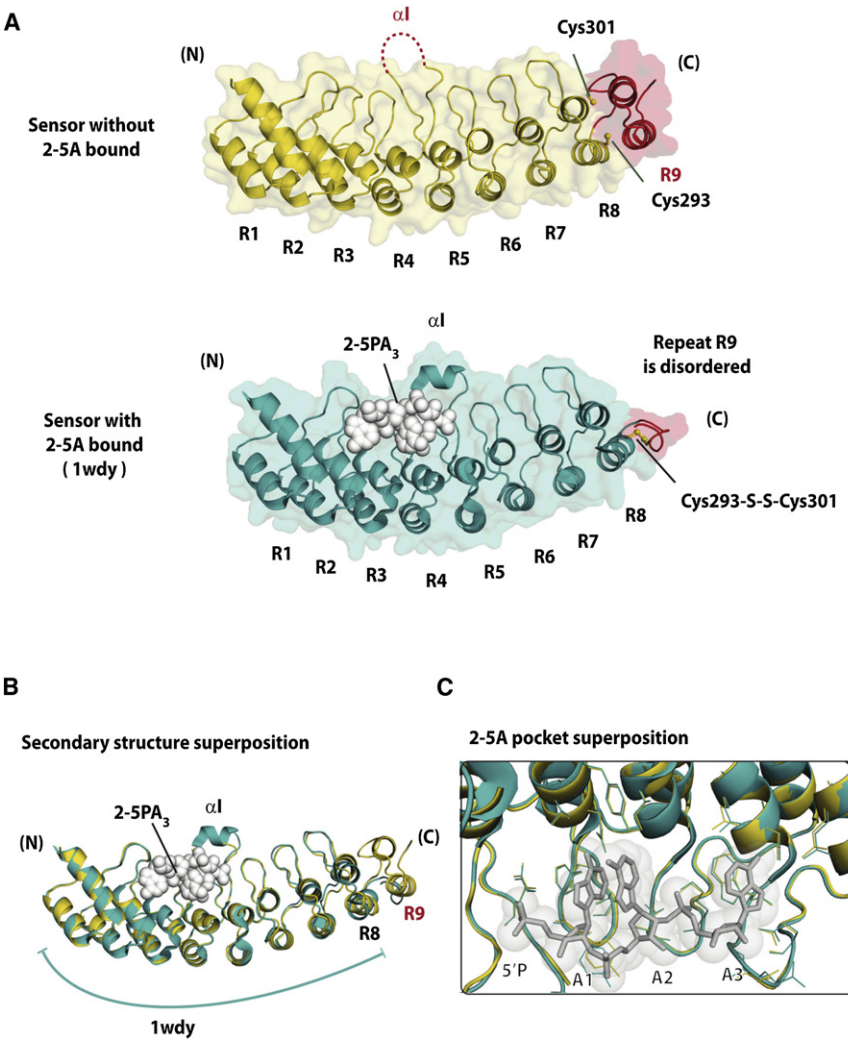

Figure 3. Structure of the Intact Sensor Domain of RNase L in the Absence of 2-5A

(A) Top: 2.4 Å crystal structure of the sensor domain of RNase L obtained without bound 2-5A. The cysteines Cys293 and Cys301 are in the reduced form, and ankyrin repeats R1-R9 are resolved. Bottom: Crystal structure 1wdy with 2-5A bound. The disulfide bridge between residues Cys293 and Cys301, and disordered ankyrin repeat R9 are shown.

(B) Superposition of the apo-structure (gold) with the structure 1wdy (cyan). Root-mean-square deviation (RMSD) = 0.319 Å.

(C) Superposition of the residues involved in binding of 2-5A in the apo-sensor and in the 2-5PA$_3$-bound structure 1wdy (RMSD = 0.195 Å). See also Figures S3 and S4, and Table S1.

concentrations, the peak shifted further and species with an apparent molecular weight (MW) exceeding that of dimer accounted for half of the signal (Figure S2F). In all experiments, discrete peaks for individual species were not detected. The absence of discrete species was observed previously with oligomeric proteins and indicates rapid equilibrium (Ahuja et al., 2004; Bitan et al., 2001; Guo et al., 2007; Nag et al., 2011). This conclusion agrees with the fast activation kinetics of RNase L described above (Figure S1C). Rapid equilibrium probably leads to underestimation of the oligomer size, as occurred with the N-terminal domain of histone deacetylase 4, which forms a tetramer but elutes as a dimer (Guo et al., 2007). The crosslinking analysis does not have limitations due to rapid equilibria, and is more suitable for detecting the dynamic oligomeric complexes of RNase L.

The ANK Domain of RNase L Is a 2-5A-Dependent Oligomerization Module

We applied the crosslinking analysis to test whether the 2-5A-binding ANK domain of RNase L contains all of the elements required for self-association. For this experiment, we expressed and purified the sensor domain of human RNase L (residues 1–337, 37 kD MW; Figure 1A). At 3 μM concentration, the sensor domain remained mostly monomeric after 20 min of crosslinking (Figure 2D). Upon addition of 2-5PA$_3$ (3 μM), monomer and dimer were observed after 30 s of crosslinking, dimer, and higher-order complexes dominated the sample after 20 min. These data show that the sensor domain of RNase L is a self-contained oligomerization device that self-associates upon 2-5A binding.

Crystal Structure of the ANK Domain in the Absence of 2-5A

To explain how 2-5A may promote self-association of the sensor domain, we examined its available cocrystal structure with 2-5PA$_3$ bound (Protein Data Bank [PDB] code 1wdy; Tanaka et al., 2004). The monomers in this structure pack via three different crystallographic interfaces (Figure S3; interfaces with mates 1, 2, and 3 are unique). The loose packing and the relatively small sizes of the crystallographic interfaces suggest that the sensor domain appears to remain monomeric upon binding of 2-5A. To explain activation of RNase L by 2-5A based on this crystal structure, it was proposed that 2-5A binding may induce a conformational change in the sensor domain (Tanaka et al., 2004).

To examine the possibility of a conformational change, we obtained the 2.4 Å crystal structure of the sensor domain in the absence of bound 2-5A (Figure 3A; Table S1). The overall protein conformation and the local conformation of the 2-5A-binding pocket are identical in the apo structure and in the reported structure with 2-5PA$_3$ bound (PDB code 1wdy; Figures 3B and 3C). This observation does not support 2-5A-induced conformational changes in the sensor domain, and suggests that it serves as a conformationally static module that regulates RNase L assembly by a different mechanism.

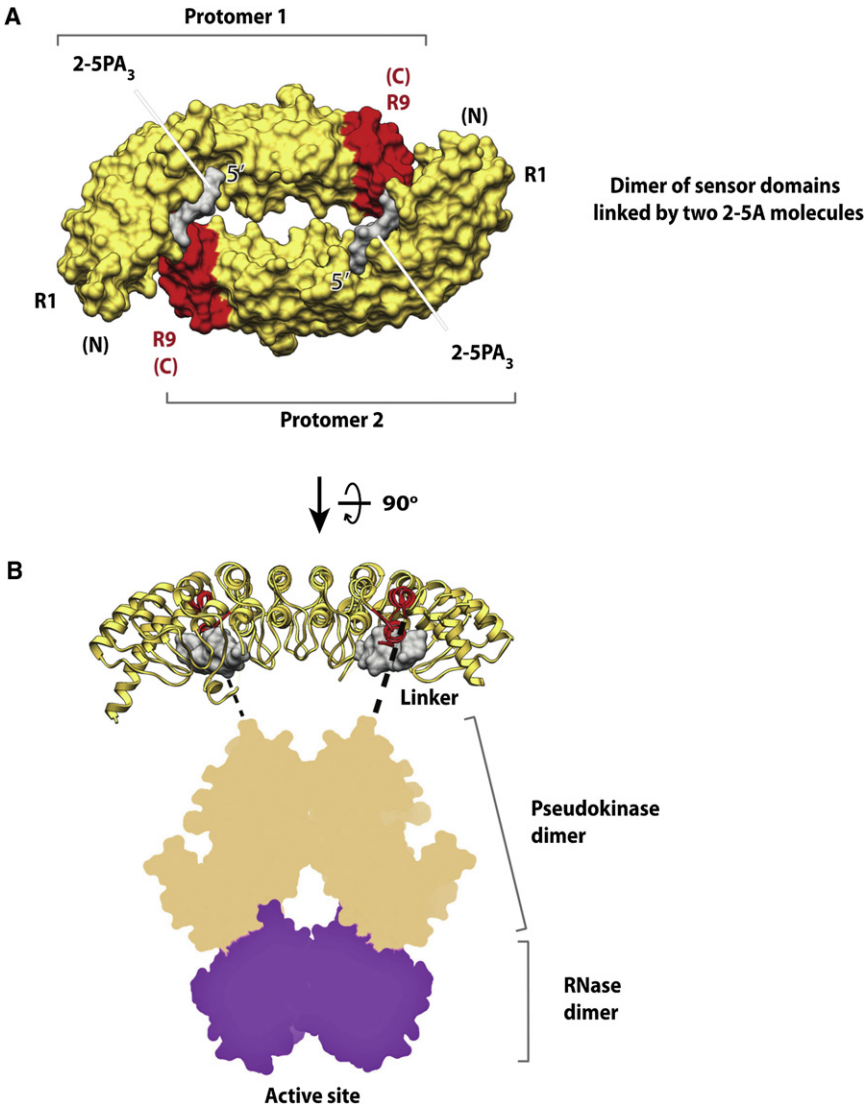

Figure 4. Structure of the 2-5A-Templated Dimer of the Sensor Domain

(A) The 2.8 Å crystal structure of the dimer formed by the sensor domains of RNase L with 2-5PA$_3$ bound. Two molecules of 2-5PA$_3$ (gray) are bound at the interface between the protomers. The dimer positions the ankyrin repeat R9 of each protomer for recognition of 2-5A bound to the partnering protomer. The ankyrin repeats R9 are colored red in both copies of the sensor domain.

(B) Model of the dimer containing all three domains of RNase L. The pseudokinase/RNase module was homology modeled using the Swiss-Model server (http://swissmodel.expasy.org). The crystal structure of Ire1 kinase/RNase (PDB code 3fbv) was used as the template. The N termini of the pseudokinase domains were aligned with the predicted location of the C termini of the sensor domains. The dimer of the sensor domains is expected to rest horizontally on the dimer of the pseudokinase/RNase domains. See also Figure S4 and Table S1.

RNase L crystallized in 1–2 days and displayed reduced Cys residues and ordered ankyrin repeat R9 (Figure 3A).

Crystal Structure of the Dimeric ANK Domain with 2-5A Bound

To understand how 2-5A drives self-association of RNase L, we aimed to cocrystallize the sensor domain with 2-5A, keeping all cysteines reduced. Screens for crystallization conditions produced cocrystals of the sensor domain with 2-5PA$_3$, 2-5PA$_4$, and 2-5HOA$_3$, which grew in 1–3 days. Cocrystals with 2-5PA$_3$ diffracted to 2.8 Å (Table S1). This crystal structure revealed a dimer of sensor domains bridged by two copies of 2-5PA$_3$ (Figure 4A). The crosslinking experiment illustrated in Figure 2D shows that the sensor domain forms not only dimers but also smaller amounts of 2-5A-induced, higher-order complexes. The crystal-packing analysis did not identify additional stable interfaces, suggesting that higher-order interfaces did not form due to competing crystal contacts. In the dimer structure, all cysteines are in their reduced form and ankyrin repeat R9 is fully ordered. The conformation of 2-5PA$_3$ is similar to that in the monomer structure 1wdy (Figure S4A); however, the sugar pucker of adenosine A3 is different (Figure S4B).

Although the structures of the apo-sensor and the 2-5PA$_3$-bound sensor domain are similar, they exhibit two local differences. First, helix αI, which is well-ordered in the cocrystal structure with 2-5PA$_3$ due to crystal packing, is disordered in the apo-structure (Figures 3A and 3B). We do not consider this difference biologically significant, because helix αI is also disordered or occupies a different position in the new crystal structure with 2-5PA$_3$ bound, as described below (Figure S3B). Second, the structure 1wdy contains only eight ankyrin repeats out of nine (R1–R8, repeat R9 is disordered) and is terminated after the repeat R8 with a short coil stabilized by a disulfide bond between cysteine residues Cys293 and Cys301 (Figure S3). The presence of a disulfide bond in a cytosolic protein RNase L is unexpected and may reflect oxidation during the 2-week crystallization period (Tanaka et al., 2004). Neither Cys is strictly conserved (Figure S3), further suggesting that the disulfide bond is not physiological. By contrast, the apo-sensor domain of

The C termini of both protomers in the dimers point in the same direction and indicate the site of attachment of the dimeric pseudokinase/RNase module. Using the crystal structure of Ire1 kinase/RNase as a template (Korennykh et al., 2009) and multiple sequence alignment-guided homology modeling (Bordoli and Schwede, 2012), we constructed the expected configuration of the dimer formed by full-length RNase L (Figure 4B). By analogy with Ire1, the pseudokinase

Cell PRESS
Open ACCESS

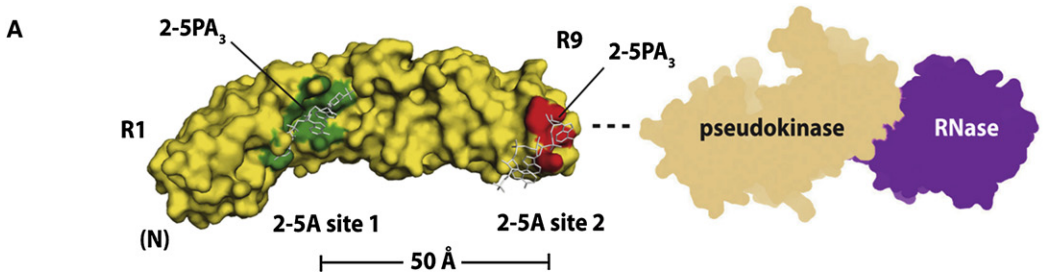

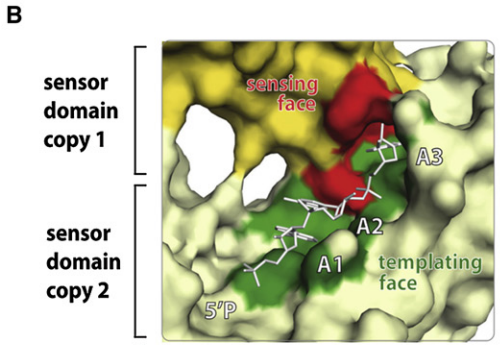

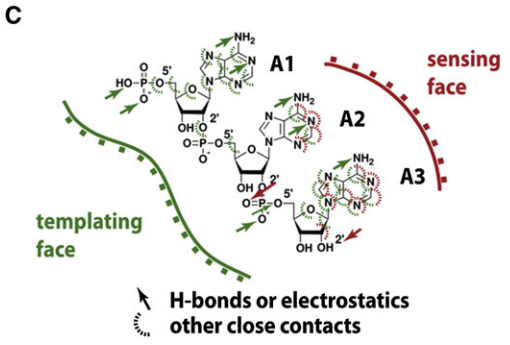

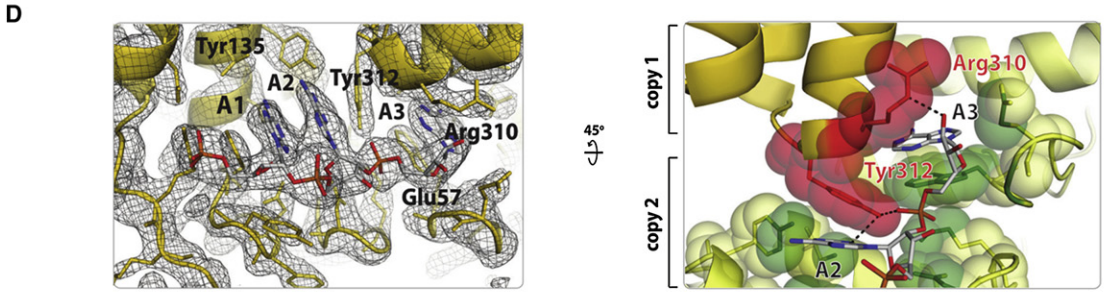

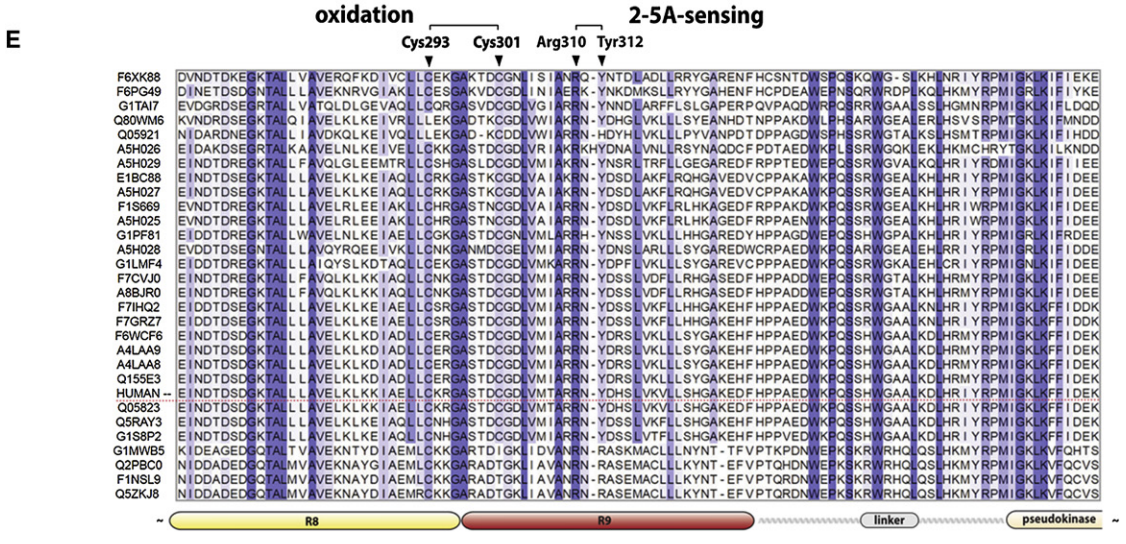

and the RNase domains are expected to form dimerization interfaces and contribute to the overall assembly of RNase L. The dimer of the sensor domains forms head-to-tail, such that the C terminus of one protomer aligns with the N terminus of a partnering protomer. In contrast, the dimer of the pseudokinase/RNase domains is expected to be head-to-head, aligning both of its N termini together. Therefore, the assembly of the full-length RNase L dimer would require a horizontal orientation of the sensor domains, as shown in the figure, to minimize the strain on the linkers between the sensor and the effector domains.

The crystal structure of the dimer revealed two independent sites for binding of 2-5A in each protomer (Figure 5A). The binding sites (sites 1 and 2) are located ~50 Å apart and recognize 2-5A via different sets of amino acids. Dimerization of the sensor domain aligns both sites in *trans*, creating a composite binding pocket for 2-5A (Figure 5B). Therefore, 2-5A promotes RNase L self-association by acting as a template that fills and completes the interface between two copies of the sensor domain. The assembled dimer binds 2-5A such that the oligonucleotide can be extended into solution from the 5′-end, explaining the ability of RNase L to become activated by longer 2-5A variants such as 2-5PA_4 (Figure 1C).

The interactions of 2-5PA_3 with site 1 involve all phosphates and adenosine bases A1, A2, and A3 (Figure 5C). The interactions with site 2 involve the adenosine bases of A2 and A3, as well as the phosphate group and the sugar moiety of adenosine A3. Adenosine A1 does not participate in the site 2 interface. Site 1 recognizes 2-5A using the same protein side chains as seen in the monomer structure (Tanaka et al., 2004). Site 2 involves ankyrin repeat R9, which was disordered in the monomer structure due to oxidation, explaining the lack of dimerization in the structure 1wdy. The backbone of ankyrin repeat R9 and side chains Arg310 and Tyr312 contact 2-5A (Figure 5D). Arg310 recognizes the nucleotide A3 via a hydrogen bond with the 2′-OH group and via a hydrophobic contact of atom Cγ with 2′C. Tyr312 forms hydrophobic and π-stacking interactions with Trp60, and hydrophobic interactions with Leu98 and Ile101 of the second protomer. Tyr312 recognizes 2-5A via polar contacts between its OH group, N3 of nucleotide A2, and nonbridging oxygen of the phosphate of A3, as well as via hydrophobic and π-stacking interactions with the nucleobases of A2 and A3 (Figure 5D). Supporting the functional role of these amino acids, Arg310 is strictly conserved, whereas Tyr312 is conserved in 24 of the ~30 known sequences of RNase L, and mutated to functionally compatible residues histidine or arginine in the six remaining sequences (Figure 5E; Supplemental Alignment).

Residues Arg310 and Tyr312 Enable Sensing of 2-5A by Human RNase L

Residues Arg310 and Tyr312 are found 38 Å and 42 Å away, respectively, from the nearest atom of 2-5PA_3 bound in the same copy of the sensor domain. To our knowledge, neither residue was previously implicated in RNase L regulation or in recognition of 2-5A. The crystal structure of the dimer (Figure 5D) positions Arg310 and Tyr312 in direct contact with 2-5PA_3 and predicts that these residues are involved in recognition. To probe these contacts, we purified full-length RNase L with Arg310Ala and Tyr312Ala point mutants, and determined their activation profiles.

Neither mutation altered the activation profile of RNase L in the absence of 2-5A (Figure 6A, magenta), suggesting that Arg310Ala and Tyr312Ala do not perturb RNase L, and that Arg310 and Tyr312 do not have roles in RNase L assembly in the absence of the activator. In the presence of 2-5PA_3 (Figure 6A, green), the Arg310Ala mutant exhibited ~10^2-fold weaker activity than wild-type (WT) RNase L and had a smaller cooperativity coefficient (n = 3.6 versus n = 5.0 for WT RNase L). Thus, the interactions between Arg310 and 2-5A facilitate recognition of 2-5A and promote assembly of larger oligomers of RNase L. The Tyr312Ala mutant failed to recognize 2-5A and exhibited indistinguishable profiles with and without 2-5PA_3 added (both reactions have a cooperativity coefficient n = 2.6; Figure 6A). Therefore, Tyr312 is strictly required for 2-5A recognition and for 2-5A-induced high-order oligomerization of RNase L. Under conditions that result in 40,000-fold activation of WT RNase L, the Arg310Ala mutant becomes activated by 500-fold and the Tyr312Ala mutant does not respond to 2-5PA_3 (Figure 6B).

To further verify that residues Arg310 and Tyr312 control the 2-5A-induced assembly of RNase L, we tested the effect of the Arg310Ala and Tyr312Ala mutations on RNase L crosslinking. WT RNase L responded to 2-5PA_3 and formed more dimers and higher-order complexes as the concentration of 2-5PA_3 was increased (Figure 6C). The Arg310Ala mutant exhibited only a small response, whereas the Tyr312Ala mutant remained unresponsive. The sensitivity of the crosslinking pattern to the point mutations designed based on the crystal structure provides an additional control that shows that our crosslinking studies describe a specific complex.

Finally, we purified the mutant versions of the sensor domain and tested their assembly in the crosslinking assay. The effects of the Arg310Ala and Tyr312Ala mutations were fully recapitulated with the sensor domain (Figure 6C). These results support the predictions from the structural analysis and independently verify the roles of Arg310 and Tyr312 in sensing 2-5A.

Figure 5. Recognition of 2-5A by the Sensor Domain of RNase L

(A) Location of two distinct binding sites for 2-5A binding in the sensor domain. Site 1 (green) is located near the N terminus, and site 2 (red) is located near the pseudokinase/RNase module. Bound 2-5A molecules are shown in white.

(B) Composite binding pocket for the adenosines A2 and A3 of 2-5PA_3 at the dimerization interface.

(C) Graphic representation of contacts between 2-5PA_3 and two 2-5A-binding sites in the sensor domains. The site 1 is larger and is expected to bind 2-5A and display it into solution for recognition by site 2.

(D) Left: σ_A-weighted electron density map $2F_{obs}$-F_{calc} for the 2-5PA_3-binding pocket in the dimer. The contour level is 1.3σ. Corresponding simulated-annealing omit maps are provided in Figure S4A. Right: Interactions of 2-5PA_3 with residues Arg310 and Tyr312 of ankyrin repeat R9.

(E) Conservation of residues Arg310 and Tyr312 in known RNase L sequences (see also Table S1 and Supplemental Alignment).

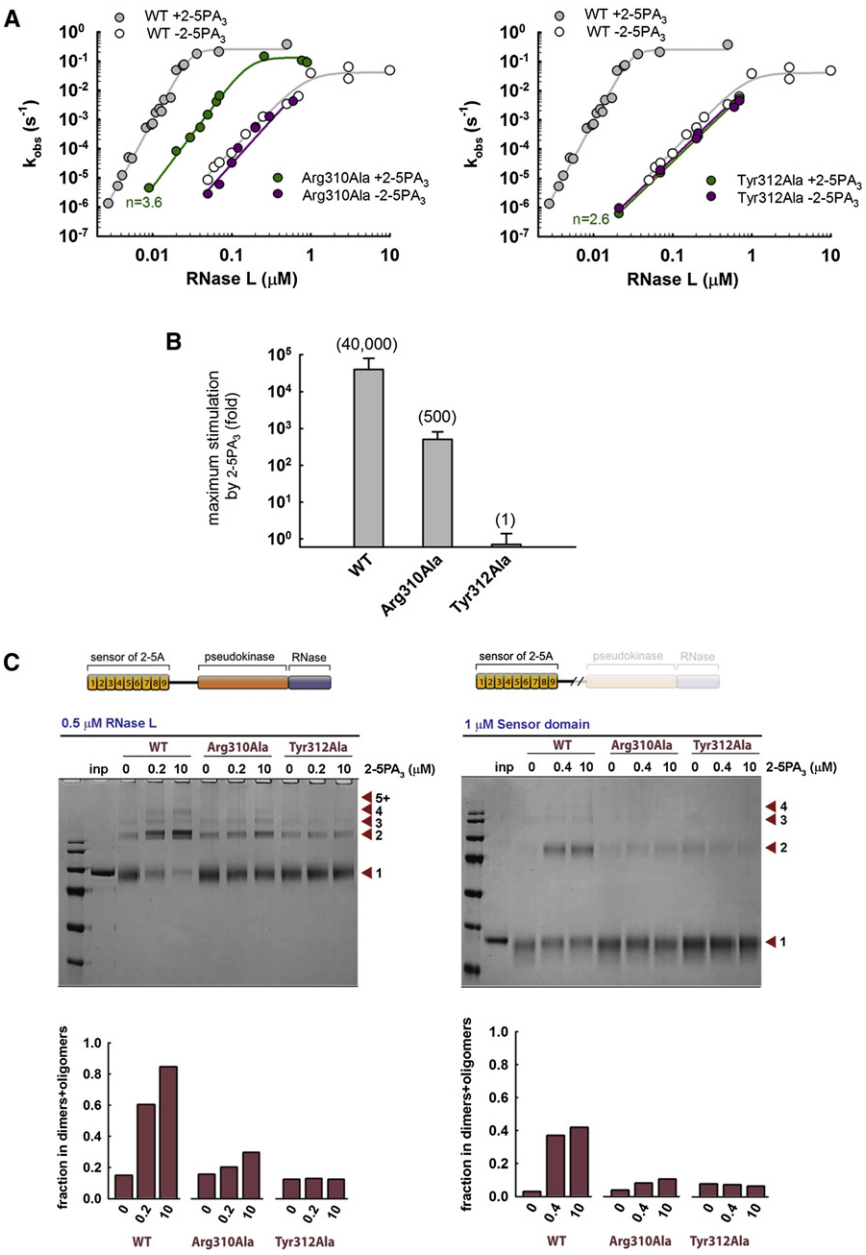

Figure 6. Residues Arg310 and Tyr312 of Ankyrin Repeat R9 Enable 2-5A Sensing

(A) Activation profiles for Arg310Ala (left) and Tyr312Ala (right) mutants of full-length RNase L obtained in the absence (magenta) and presence (green) of 2-5PA_3. Corresponding profiles of WT RNase L from Figure 1B are overlaid for comparison (gray).

(B) Maximum response of WT, Arg310Ala, and Tyr312Ala RNase L to 2-5PA_3 determined from data in (A). Bars show uncertainties in response defined from propagated errors of k_{obs} measurements.

(C) 2-5PA_3-induced self-assembly of WT, Arg310Ala, and Tyr312Ala RNase L visualized by chemical crosslinking with glutaraldehyde. Profiles for full-length RNase L (left) and the sensor domain (right; residues 1–337) are shown. Bar charts show gel quantitation.

DISCUSSION

Here we describe high-order oligomerization in the 2-5A/RNase L system and establish the molecular mechanism by which 2-5A activates RNase L. Two copies of 2-5A simultaneously connect two RNase L monomers using residues Arg310 and Tyr312 in the ANK domain. This mechanism creates RNase L dimers and provides building blocks for higher-order oligomers that ultimately cleave RNA (Figure 7).

By analogy with the phylogenetically related transmembrane kinase/RNase Ire1 in the ER stress response (Korennykh et al., 2009), the oligomers of RNase L should be stabilized by pseudokinase/pseudokinase and RNase/RNase interfaces, in addition to the sensor/$(2\text{-}5A)_2$/sensor interface specific to RNase L. Although our studies of the purified pseudokinase/RNase domains were hindered by nonspecific aggregation of the constructs tested, the contribution to oligomerization from the pseudokinase/RNase module of RNase L was supported experimentally by the observation of higher oligomers and faster crosslinking with full-length RNase L than with purified sensor domain (compare 2 min time points in Figure 2B versus 2D). The high-order assembly of RNase L is poised to provide a vast surface for interaction with additional factors and may establish a signaling platform in the IFN response with functions that remain to be fully defined.

The cooperative activation of RNase L and its position within a positive feedback loop (Ireland et al., 2009) suggest that RNase L may serve as an ultrasensitive amplification device in the IFN response. The cooperativity coefficients for RNase L self-association and for binding of 2-5A (Figures 1B and 1C) indicate that the signaling activity of RNase L should increase by up to 4-fold (2^n, n = 2) for a 2-fold induction of 2-5A, and by up to 32-fold (2^n, n = 5) for a 2-fold induction of RNase L expression levels. These estimates suggest that a relatively small upregulation of RNase L by IFNs in human cells (Zhou et al., 2005) could nevertheless produce large RNA cleavage outputs. The high-order assembly of RNase L should allow a robust response early upon virus infection without a delay to synthesize large concentrations of 2-5A needed for a less cooperative sensor. The same phenomenon should ensure a more complete, switch-like shutdown of RNase L at low levels of 2-5A. Steep deactivation of RNase L at low 2-5A concentrations should protect cellular RNA from rogue RNase L activity

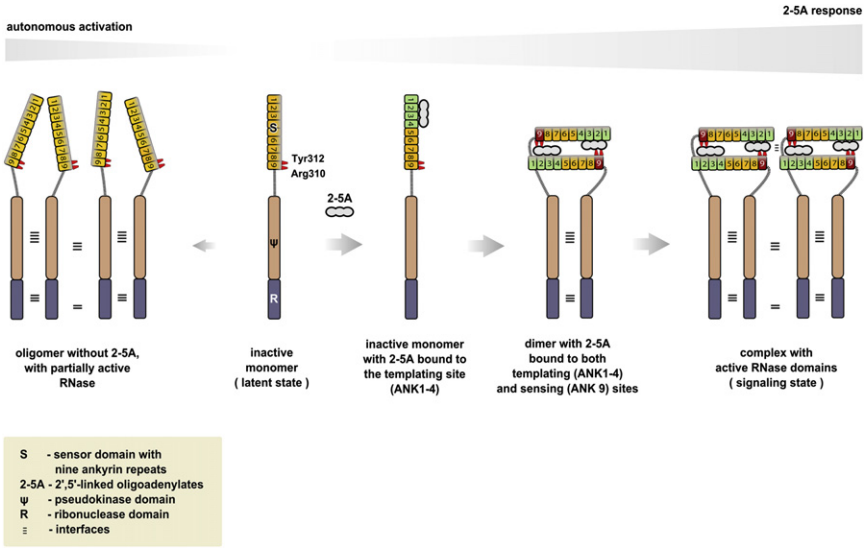

Figure 7. Model of RNase L Activation by 2-5A-Induced High-Order Assembly

RNase L undergoes 2-5A-dependent and -independent activation. The binding of two molecules of 2-5A to the N-terminal sensor domain stabilizes the dimeric state of RNase L and supplies the structural units for the catalytically active high-order oligomers.

and allow RNase L storage in the cytosol without undue RNA degradation until viral infection is detected.

The binding of 2-5A has been considered a prerequisite for RNase L activation (Dong and Silverman, 1997). We now show that the requirement for 2-5A binding is mostly bypassed at micromolar concentrations of RNase L (Figure 1B). The physiological role of the 2-5A-independent activation of RNase L is unknown. Although the intracellular concentrations of RNase L may never reach 1 μM, the ability of RNase L to become active without 2-5A suggests that templating or scaffolding factors could modulate RNase L and allow as yet unidentified scenarios when its signaling is uncoupled from the IFN response and becomes committed to alternative cellular programs.

RNase L detects 2-5A via ankyrin repeats, a very common motif in eukaryotic proteins found in up to 3%–4% of human protein genes (Hunter et al., 2012). Among other functions, ankyrin repeats mediate protein-protein interactions during cell adhesion (Chiswell et al., 2010), endocytosis (Tanno et al., 2012), development (Tee and Peppelenbosch, 2010), and death (Bialik et al., 2004). Our data expand the mapped repertoire of ankyrin repeats and show that they can serve as homo-oligomerization modules that sense a nucleic acid ligand and drive the association of attached functional domains. It is possible that nucleic acid-mediated homo-oligomerization is not limited to the sensor domain of RNase L and applies to other ankyrin-bearing proteins.

EXPERIMENTAL PROCEDURES

Experimental Errors

Rate constants and cooperativity coefficients were determined from multiple measurements and reproduced on different days. The rate variations between measurements done on different days were typically within 2-fold and were small compared with the effects we studied.

Expression and Purification of WT and Mutant RNase L

Full-length human RNase L was cloned into the pGEX-6P-2 vector, which was previously used for expression of Ire1 (Korennykh et al., 2009). DNA primers for cloning and mutagenesis were designed in Biochem Lab Solutions ELN (http://biochemlabsolutions.com/ELN/ELN.html) and purchased from IDT. Proteins were expressed in *Escherichia coli*. Expression and purification were conducted as described previously for Ire1 (Carroll et al., 1997). Protein concentrations were determined from UV spectra in 6 M guanidinium chloride solution containing 50 mM sodium phosphate (pH 6.5), using absorbance at 280 nm. Extinction coefficients were derived from RNase L protein sequence in the Lab Tools module of Biochem Lab Solutions ELN. Stocks of purified RNase L were concentrated to 10–20 mg/ml and stored at −80°C. The RNase L used in this work was ≥99% pure, as judged by fast protein liquid chromatography and Coomassie blue staining.

RNA Substrates

RNA 21-mer $C_{11}U_3C_7$ was synthesized by Dharmacon Inc. The oligonucleotide was purified by denaturing (8 M urea) 15% PAGE. Polyacrylamide (40%, crosslinked 29:1) was purchased from National Diagnostics. RNA concentration was determined in RNase-free water using extinction coefficients calculated from the RNA sequence in Biochem Lab Solutions ELN. RNA was labeled with ^{32}P at the 5′-terminus using T4 PNK (NEB) and $\gamma^{32}P$-ATP (Perkin Elmer). All ^{32}P-labeled substrates were purified by denaturing 15% PAGE. RNA was stored at −20°C in buffer containing 20 mM HEPES (pH 7.4), 100 mM NaCl, and 1 mM $Mg(OAc)_2$.

2-5A

5′-OH-$A_{2′,5′}A_{2′,5′}A$ (2-5HOA$_3$), 5′-P-$A_{2′,5′}A_{2′,5′}A$ (2-5PA$_3$), and 5′-P-$A_{2′,5′}A_{2′,5′}A_{2′,5′}A$ (2-5PA$_4$) were synthesized by solid-phase synthesis at ChemGenes. Purity was ≥98% by capillary electrophoresis conducted by ChemGenes.

RNase L Cleavage Assay

RNA cleavage reactions were conducted at 20°C in buffer containing 20 mM HEPES (pH 7.4 at 20°C), 70 mM NaCl, 2 mM $Mg(OAc)_2$, 4 mM dithiothreitol (DTT), 10% glycerol, <1 nM ^{32}P-labeled RNA substrate, and human purified RNase L as indicated for each experiment. Then 1 μl of RNA was added to 9 μl of a preincubated reaction mixture containing all components except RNA substrate. At time intervals, 1-μl aliquots were withdrawn from each reaction tube into 6 μl of stop solution containing 10 M urea, 0.01% xylene cyanol, and 0.01% bromophenol blue. The samples were separated by denaturing 15% PAGE and exposed on a phosphor storage screen. The screens were scanned on Typhoon FLA-7000 and quantified using http://biochemlabsolutions.com/GelQuantNET.html 1.7 gel analysis software (http://biochemlabsolutions.com). The data were analyzed using SigmaPlot as described previously (Korennykh et al., 2009, 2011). Briefly, cooperative activation profiles in Figure 1B were fit to the Hill equation; cooperative profiles in Figure 1C were fit to the Hill equation with an added constant that accounts for the rates in the absence of 2-5A.

Crosslinking Analysis

Samples of RNase L in 45 μl reaction buffer (20 mM HEPES pH 7.4, 70 mM NaCl, 2 mM $Mg(OAc)_2$, 4 mM DTT, 5% glycerol) were mixed with 5 μl of fresh 50 mM glutaraldehyde solution. Reactions were incubated at 20°C. Aliquots

(10 μl) were withdrawn into 6 μl of stop solution (80 μl NuPage SDS 4× protein loading dye, 30 μl 200 mM glycine, and 20 μl 1 M DTT). Quenched aliquots were boiled and loaded on a 10% Bis-Tris PAGE (NuPage). Gels were stained with Coomassie blue G-250. The oligomer band sizes were measured using the http://biochemlabsolutions.com/GelQuantNET.html gel ruler tool.

Protein and Protein●2-5A Complex Crystallization

The sensor domain of RNase L (10 mg/ml in buffer containing 150 mM NaCl, 20 mM HEPES pH 7.4, 1 mM DTT, and 2% glycerol) was crystallized either without ligands or as a complex with 2-5A. Crystals of the apo-sensor domain grew from 50 mM potassium acetate, 20% PEG3350 solution during 2–3 days at room temperature and formed rectangular prisms. Crystals of complexes with 2-5HOA$_3$, 2-5PA$_3$, and 2-5PA$_4$ grew from 200 mM sodium acetate and 18% PEG 3350, and from 1.3 M sodium citrate. Only cocrystals grown with 2-5PA$_3$ were suitable for diffraction analysis. For data collection, crystals were cryoprotected in well solutions supplemented with 25%–30% ethylene glycol.

Data Collection and Analysis

X-ray diffraction data were recorded on beamline X29 at Brookhaven National Laboratory (Upton, NY). The data sets were collected using an X-ray wavelength of 1.075 Å and an oscillation angle of 1°. The data were indexed, integrated, and scaled in XDS. Five percent of the reflections were marked as a test set. Molecular replacement solutions were found with the use of PHASER (McCoy et al., 2007) and PDB entry 1wdy as a search model. Crystals of the apo-sensor domain belong to space group $P2_12_12_1$ and contain two molecules in asymmetric unit. Crystals of the complex between the sensor domain and 2-5PA$_3$ belong to space group $P2_1$ and contain four molecules in asymmetric unit. Following initial rigid-body refinement in PHENIX (Adams et al., 2002), the structures were built in Coot (Emsley and Cowtan, 2004) and refined using simulated annealing (2,000 K) and TLS refinement in PHENIX (Adams et al., 2002). The structure without 2-5PA$_3$ bound in space group $P2_12_12_1$ was refined without the use of NCS, which resulted in a lower R_{free} than with 2-fold NCS enabled. The complex with 2-5PA$_3$ in space group $P2_1$ was refined with NCS constraints. One NCS group was comprised of one sensor monomer. Fourier F_{obs}-F_{calc} difference maps were used for interpretation of new electron density. Final structures were visualized in PyMol 1.2 (DeLano Scientific, LLC). The resulting models had good stereochemical parameters, no Ramachandran outliers, and low crystallographic R/R_{free} = 0.217/0.249 for the apo-structure and R/R_{free} = 0.228/0.261 for the sensor●2-5PA$_3$ complex (Table S1).

ACCESSION NUMBERS

The coordinates and the structure factors reported in this work have been deposited in the PDB under ID codes 4G8K and 4G8L (http://www.rcsb.org/).

SUPPLEMENTAL INFORMATION

Supplemental Information includes four figures, one table, and a supplemental alignment and can be found with this article online at http://dx.doi.org/10.1016/j.celrep.2012.09.004.

LICENSING INFORMATION

ACKNOWLEDGMENTS

We are grateful to Fred Hughson (Princeton University), Andrei Korostelev (University of Massachusetts, Worcester), and Peter Walter (University of California, San Francisco) for critically reading the manuscript. We thank the staff of Brookhaven National Laboratory and Phil Jeffrey for help at beamline X29. Y.H. prepared RNase L expression constructs, produced recombinant sensor domains and pseudokinase/RNase domains, and conducted crystallization of the apo-sensor domain. J.D. expressed and purified RNase L. J.D. and Y.H. conducted size-exclusion studies. G.W. expressed and purified full-length RNase L and RNase L mutants. A.K. supervised the work, conducted the solution studies, cocrystallized sensor domain with 2-5A, and solved the crystal structures. A.K. wrote the manuscript.

Received: June 10, 2012
Revised: July 23, 2012
Accepted: September 7, 2012
Published online: October 18, 2012

REFERENCES

Adams, P.D., Grosse-Kunstleve, R.W., Hung, L.W., Ioerger, T.R., McCoy, A.J., Moriarty, N.W., Read, R.J., Sacchettini, J.C., Sauter, N.K., and Terwilliger, T.C. (2002). PHENIX: building new software for automated crystallographic structure determination. Acta Crystallogr. D Biol. Crystallogr. *58*, 1948–1954.

Ahuja, A., Purcarea, C., Ebert, R., Sadecki, S., Guy, H.I., and Evans, D.R. (2004). Aquifex aeolicus dihydroorotase: association with aspartate transcarbamoylase switches on catalytic activity. J. Biol. Chem. *279*, 53136–53144.

Bialik, S., Bresnick, A.R., and Kimchi, A. (2004). DAP-kinase-mediated morphological changes are localization dependent and involve myosin-II phosphorylation. Cell Death Differ. *11*, 631–644.

Bitan, G., Lomakin, A., and Teplow, D.B. (2001). Amyloid beta-protein oligomerization: prenucleation interactions revealed by photo-induced cross-linking of unmodified proteins. J. Biol. Chem. *276*, 35176–35184.

Bordoli, L., and Schwede, T. (2012). Automated protein structure modeling with SWISS-MODEL Workspace and the Protein Model Portal. Methods Mol. Biol. *857*, 107–136.

Carroll, S.S., Chen, E., Viscount, T., Geib, J., Sardana, M.K., Gehman, J., and Kuo, L.C. (1996). Cleavage of oligoribonucleotides by the 2′,5′-oligoadenylate-dependent ribonuclease L. J. Biol. Chem. *271*, 4988–4992.

Carroll, S.S., Cole, J.L., Viscount, T., Geib, J., Gehman, J., and Kuo, L.C. (1997). Activation of RNase L by 2′,5′-oligoadenylates. Kinetic characterization. J. Biol. Chem. *272*, 19193–19198.

Chakrabarti, A., Jha, B.K., and Silverman, R.H. (2011). New insights into the role of RNase L in innate immunity. J. Interferon Cytokine Res. *31*, 49–57.

Chiswell, B.P., Stiegler, A.L., Razinia, Z., Nalibotski, E., Boggon, T.J., and Calderwood, D.A. (2010). Structural basis of competition between PINCH1 and PINCH2 for binding to the ankyrin repeat domain of integrin-linked kinase. J. Struct. Biol. *170*, 157–163.

Cole, J.L., Carroll, S.S., and Kuo, L.C. (1996). Stoichiometry of 2′,5′-oligoadenylate-induced dimerization of ribonuclease L. A sedimentation equilibrium study. J. Biol. Chem. *271*, 3979–3981.

Cole, J.L., Carroll, S.S., Blue, E.S., Viscount, T., and Kuo, L.C. (1997). Activation of RNase L by 2′,5′-oligoadenylates. Biophysical characterization. J. Biol. Chem. *272*, 19187–19192.

Cornell, R. (1989). Chemical cross-linking reveals a dimeric structure for CTP:phosphocholine cytidylyltransferase. J. Biol. Chem. *264*, 9077–9082.

Domingo-Gil, E., González, J.M., and Esteban, M. (2010). Identification of cellular genes induced in human cells after activation of the OAS/RNaseL pathway by vaccinia virus recombinants expressing these antiviral enzymes. J. Interferon Cytokine Res. *30*, 171–188.

Dong, B., and Silverman, R.H. (1995). 2-5A-dependent RNase molecules dimerize during activation by 2-5A. J. Biol. Chem. *270*, 4133–4137.

Dong, B., and Silverman, R.H. (1997). A bipartite model of 2-5A-dependent RNase L. J. Biol. Chem. *272*, 22236–22242.

Dong, B., Niwa, M., Walter, P., and Silverman, R.H. (2001). Basis for regulated RNA cleavage by functional analysis of RNase L and Ire1p. RNA *7*, 361–373.

Emsley, P., and Cowtan, K. (2004). Coot: model-building tools for molecular graphics. Acta Crystallogr. D Biol. Crystallogr. *60*, 2126–2132.

Fabre, O., Salehzada, T., Lambert, K., Boo Seok, Y., Zhou, A., Mercier, J., and Bisbal, C. (2012). RNase L controls terminal adipocyte differentiation, lipids storage and insulin sensitivity via CHOP10 mRNA regulation. Cell Death Differ. *19*, 1470–1481.

Guo, L., Han, A., Bates, D.L., Cao, J., and Chen, L. (2007). Crystal structure of a conserved N-terminal domain of histone deacetylase 4 reveals functional insights into glutamine-rich domains. Proc. Natl. Acad. Sci. USA *104*, 4297–4302.

Hartmann, R., Justesen, J., Sarkar, S.N., Sen, G.C., and Yee, V.C. (2003). Crystal structure of the 2′-specific and double-stranded RNA-activated interferon-induced antiviral protein 2′-5′-oligoadenylate synthetase. Mol. Cell *12*, 1173–1185.

Hayer-Hartl, M.K., Martin, J., and Hartl, F.U. (1995). Asymmetrical interaction of GroEL and GroES in the ATPase cycle of assisted protein folding. Science *269*, 836–841.

Hunter, S., Jones, P., Mitchell, A., Apweiler, R., Attwood, T.K., Bateman, A., Bernard, T., Binns, D., Bork, P., Burge, S., et al. (2012). InterPro in 2011: new developments in the family and domain prediction database. Nucleic Acids Res. *40*(Database issue), D306–D312.

Ireland, D.D., Stohlman, S.A., Hinton, D.R., Kapil, P., Silverman, R.H., Atkinson, R.A., and Bergmann, C.C. (2009). RNase L mediated protection from virus induced demyelination. PLoS Pathog. *5*, e1000602.

Jha, B.K., Polyakova, I., Kessler, P., Dong, B., Dickerman, B., Sen, G.C., and Silverman, R.H. (2011). Inhibition of RNase L and RNA-dependent protein kinase (PKR) by sunitinib impairs antiviral innate immunity. J. Biol. Chem. *286*, 26319–26326.

Jiang, F., Ramanathan, A., Miller, M.T., Tang, G.Q., Gale, M., Jr., Patel, S.S., and Marcotrigiano, J. (2011). Structural basis of RNA recognition and activation by innate immune receptor RIG-I. Nature *479*, 423–427.

Korennykh, A.V., Egea, P.F., Korostelev, A.A., Finer-Moore, J., Zhang, C., Shokat, K.M., Stroud, R.M., and Walter, P. (2009). The unfolded protein response signals through high-order assembly of Ire1. Nature *457*, 687–693.

Korennykh, A.V., Egea, P.F., Korostelev, A.A., Finer-Moore, J., Stroud, R.M., Zhang, C., Shokat, K.M., and Walter, P. (2011). Cofactor-mediated conformational control in the bifunctional kinase/RNase Ire1. BMC Biol. *9*, 48.

Luthra, P., Sun, D., Silverman, R.H., and He, B. (2011). Activation of IFN-β expression by a viral mRNA through RNase L and MDA5. Proc. Natl. Acad. Sci. USA *108*, 2118–2123.

Maier, C., Haeusler, J., Herkommer, K., Vesovic, Z., Hoegel, J., Vogel, W., and Paiss, T. (2005). Mutation screening and association study of RNASEL as a prostate cancer susceptibility gene. Br. J. Cancer *92*, 1159–1164.

Malathi, K., Dong, B., Gale, M., Jr., and Silverman, R.H. (2007). Small self-RNA generated by RNase L amplifies antiviral innate immunity. Nature *448*, 816–819.

Manning, G., Whyte, D.B., Martinez, R., Hunter, T., and Sudarsanam, S. (2002). The protein kinase complement of the human genome. Science *298*, 1912–1934.

McCoy, A.J., Grosse-Kunstleve, R.W., Adams, P.D., Winn, M.D., Storoni, L.C., and Read, R.J. (2007). Phaser crystallographic software. J. Appl. Cryst. *40*, 658–674.

Mischke, R., Kleemann, R., Brunner, H., and Bernhagen, J. (1998). Cross-linking and mutational analysis of the oligomerization state of the cytokine macrophage migration inhibitory factor (MIF). FEBS Lett. *427*, 85–90.

Mullan, P.B., Hosey, A.M., Buckley, N.E., Quinn, J.E., Kennedy, R.D., Johnston, P.G., and Harkin, D.P. (2005). The 2,5 oligoadenylate synthetase/RNaseL pathway is a novel effector of BRCA1- and interferon-gamma-mediated apoptosis. Oncogene *24*, 5492–5501.

Nag, S., Sarkar, B., Bandyopadhyay, A., Sahoo, B., Sreenivasan, V.K., Kombrabail, M., Muralidharan, C., and Maiti, S. (2011). Nature of the amyloid-beta monomer and the monomer-oligomer equilibrium. J. Biol. Chem. *286*, 13827–13833.

Naik, S., Paranjape, J.M., and Silverman, R.H. (1998). RNase L dimerization in a mammalian two-hybrid system in response to 2′,5′-oligoadenylates. Nucleic Acids Res. *26*, 1522–1527.

Sadler, A.J., and Williams, B.R. (2008). Interferon-inducible antiviral effectors. Nat. Rev. Immunol. *8*, 559–568.

Silverman, R.H., Jung, D.D., Nolan-Sorden, N.L., Dieffenbach, C.W., Kedar, V.P., and SenGupta, D.N. (1988). Purification and analysis of murine 2-5A-dependent RNase. J. Biol. Chem. *263*, 7336–7341.

Tanaka, N., Nakanishi, M., Kusakabe, Y., Goto, Y., Kitade, Y., and Nakamura, K.T. (2004). Structural basis for recognition of 2′,5′-linked oligoadenylates by human ribonuclease L. EMBO J. *23*, 3929–3938.

Tanno, H., Yamaguchi, T., Goto, E., Ishido, S., and Komada, M. (2012). The Ankrd 13 family of UIM-bearing proteins regulates EGF receptor endocytosis from the plasma membrane. Mol. Biol. Cell *23*, 1343–1353.

Tee, J.M., and Peppelenbosch, M.P. (2010). Anchoring skeletal muscle development and disease: the role of ankyrin repeat domain containing proteins in muscle physiology. Crit. Rev. Biochem. Mol. Biol. *45*, 318–330.

Zhou, A., Molinaro, R.J., Malathi, K., and Silverman, R.H. (2005). Mapping of the human RNASEL promoter and expression in cancer and normal cells. J. Interferon Cytokine Res. *25*, 595–603.